

Solution of the Inverse Jet in a Crossflow Problem by a Predictor-Corrector Technique

Joseph R VanderVeer, Yogesh Jaluria*

*Department of Mechanical and Aerospace Engineering: Rutgers University, 98 Brett Rd,
Piscataway NJ, 08854*

Abstract

Keywords: Inverse Problems, Computational Heat Transfer, Convection

1. Introduction

Thermal-fluid systems often create situations where the engineering problem is an inverse heat transfer problem. These problems often have limited physical access, very limited to no boundary condition knowledge, and/or limited domain knowledge.

For example, the temperature distribution of an optical fiber drawing furnace is difficult to measure directly due to shape, inaccessibility, and high temperatures. The center of the furnace is easily accessible and this directly leads to an inverse heat transfer problem. Issa et al. [1] developed a regularization technique utilizing the centerline temperature from which the wall temperature may be obtained.

Another example, is the inverse plume in a crossflow problem. The problem entails solving for the plume boundary conditions utilizing limited domain knowledge. A novel predictor-corrector method was developed by VanderVeer and Jaluria [2] to solve such a problem. The method requires a specific pattern of known points to match exactly to predict the inverse solution. The specific pattern was optimized to require the least number of known points for plume in a crossflow problem [3]. With zero error in the

*Corresponding Author

Email address: jaluria@soemail.rutgers.edu (Yogesh Jaluria)

Nomenclature

\mathbf{r}	vector location of sampled points	δ	vector distance between the actual sampled location and the current test location
a	number of sample locations used in the predictor stage	λ	thermal conductivity
b, m	model parameters	μ	dynamic viscosity
$C_1, C_2, C_{1\epsilon}, C_\mu, \sigma_k, \sigma_\epsilon$	$k - \epsilon$ model coefficients	μ_t	eddy viscosity
d	number of simulations	ϕ	normalized temperature $\phi = \frac{T-T_\infty}{T_S-T_\infty}$
E	thermal energy	ρ	density
F	minimization function	ε	error associated with the inverse convection method at a location with given sampled data
k, ϵ	turbulence kinetic energy, dissipation rate		
l, I	turbulence length scale and intensity		
n	number of sample locations		
P	pressure		
P_{rt}	turbulent Prandtl number		
T	temperature		
t	time		
U	free stream velocity		
X, Y	normalized coordinates		
x, y	coordinates		
Greek Symbols		Superscripts	
Δ	relative difference between the first sampled point and other sampled points	$*$	predictor stage, alternative heat flux eqn.
		Subscripts	
		$0, 1, 2$	sample point indexes
		∞	free stream
		A, B	data set A,B
		i, j, k	index
		mod	modified
		O	optimized
		P	predicted
		S	source

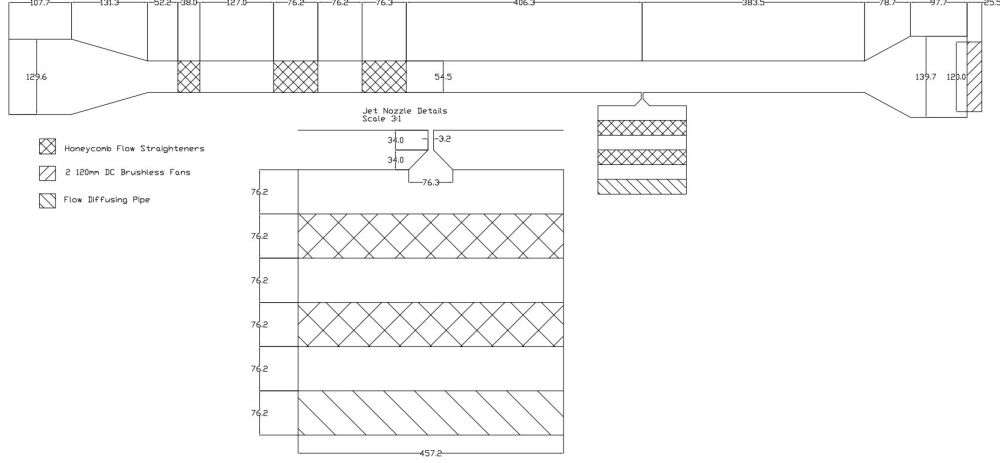


Figure 1: Schematics of the wind tunnel and jet

data a minimum of three known points was possible, but small amounts of error would require the known point count to increase to at least five.

The present work is the logical progression of the inverse plume in a crossflow problem, the inverse jet in a crossflow problem. The inverse jet in a crossflow problem has many more practical applications such as exhaust stacks and fuel injection systems. The previous technique will be modified to meet the needs of the new problem.

2. Experimental System

The experiment consists of a wind tunnel with a surface level jet located within the test section. The jet uses compressed air passed through flow straighteners to achieve a velocity of U_S and is heated to temperature T_S . The jet is subjected to a perpendicular crossflow of velocity U_∞ . Figure 1 is a diagram of the wind tunnel and jet, dimensions are in millimeters.

The wind tunnel test section dimensions are $54.5 \times 305 \times 254 \text{ mm}$. The maximum velocity of the wind tunnel is 5.0 m/s . The jet is heated by electric cartridge heaters (Omega AHP-7561) with a maximum temperature of 425 K due to material limitations of the wind tunnel. The X-direction is directed downstream of the wind tunnel with the zero at the center of the jet. The Y-direction is in the direction of the jet and is zero at the surface of the wind

tunnel. Due to the large aspect ratio of the wind tunnel the flow is assumed to be two-dimensional.

The free stream velocity is determined by a Pitot-Static tube attached to a NIST traceable differential pressure sensor from Omega(PX655-0.1DI). The pressure sensor has a full scale reading of 0.1 inches of water and is accurate to 0.05% of full scale. This results in a maximum of 3% error of the calculated velocity.

The jet velocity is determined utilizing a rotameter and verified using a Pitot-Static tube attached to the same previously described pressure sensor. This results in the same amount of error of 3% for the jet velocity.

The temperature of domain is measured using a K-type thermocouple mounted to an X-Y traversing stage. Sampled data over the course of several days indicate repeatability of the experiment to within 2%.

3. Numerical Simulations

The simulations were all performed using Ansys Fluent[4]. The Navier-Stokes equations were solved using a three-dimensional, steady state, realizable $k - \epsilon$ model with enhanced wall effects. Conjugate heat transfer is modelled. The free stream Reynolds number is of order 6×10^3 , while the jet Reynolds number is between 10^3 and 10^4 . The Rayleigh number is of order 10^7 .

The governing equations are expressed below:

$$u_i = \overline{u_i} + u'_i \quad (1)$$

$$\frac{\partial \rho}{\partial t} + \frac{\partial}{\partial x_i} (\rho u_i) = 0 \quad (2)$$

$$\begin{aligned} \frac{\partial}{\partial t} (\rho u_i) + \frac{\partial}{\partial x_j} (\rho u_i u_j) = \\ \frac{\partial P}{\partial x_i} + \frac{\partial}{\partial x_j} \left[\mu \left(2S_{ij} - \frac{2}{3} \delta_{ij} \frac{\partial u_k}{\partial x_k} \right) - \overline{\rho u'_i u'_j} \right] \end{aligned} \quad (3)$$

$$\begin{aligned} \frac{\partial}{\partial t} (\rho E) + \frac{\partial}{\partial x_i} [u_i (\rho E + P)] = \\ \frac{\partial}{\partial x_i} \left[\left(\lambda + \frac{C_p \mu_t}{Pr_t} \right) \frac{\partial T}{\partial x_i} \right] \end{aligned} \quad (4)$$

$$\begin{aligned}
\frac{\partial}{\partial t}(\rho k) + \frac{\partial}{\partial x_j}(\rho k u_j) = \\
\frac{\partial}{\partial x_j} \left[\left(\mu + \frac{\mu_t}{\sigma_k} \right) \frac{\partial k}{\partial x_j} \right] + \frac{\partial u_j}{\partial x_i} \left(-\rho \overline{u'_i u'_j} \right) \\
- g_i \frac{\mu_t}{\rho P_{rt}} \frac{\partial \rho}{\partial x_i} + \rho \epsilon
\end{aligned} \tag{5}$$

$$\begin{aligned}
\frac{\partial}{\partial t}(\rho \epsilon) + \frac{\partial}{\partial x_j}(\rho \epsilon u_j) = \\
\frac{\partial}{\partial x_j} \left[\left(\mu + \frac{\mu_t}{\sigma_\epsilon} \right) \frac{\partial \epsilon}{\partial x_j} \right] + \rho C_1 S \epsilon - \rho C_2 \frac{\epsilon^2}{k + \sqrt{\nu \epsilon}} \\
- C_{1\epsilon} \frac{\epsilon}{k} C_{3\epsilon} g_i \frac{\mu_t}{\rho P_{rt}} \frac{\partial \rho}{\partial x_i}
\end{aligned} \tag{6}$$

$$- \rho \overline{u'_i u'_j} = 2\mu_t S_{ij} - \frac{2}{3} \delta_{ij} \left(\rho k + \mu_t \frac{\partial u_k}{\partial x_k} \right) \tag{7}$$

The constants for the turbulence model are [5, 6] :

$$C_{1\epsilon} = 1.44, C_2 = 1.9, \sigma_k = 1.0, \sigma_\epsilon = 1.2, P_{rt} = 0.85 \tag{8}$$

$$C_1 = \max \left[0.43, \frac{Sk/\epsilon}{Sk/\epsilon + 5} \right], S = \sqrt{2S_{ij}S_{ji}}, C_{3\epsilon} = \tanh \left(\frac{u_g}{u_p} \right) \tag{9}$$

$$\mu_t = \frac{\rho C_\mu k^2}{\epsilon} \tag{10a}$$

$$C_\mu = \frac{1}{A_0 + \frac{A_1 k U^*}{\epsilon}} \tag{10b}$$

$$U^* \equiv \sqrt{S_{ij}S_{ji} + \Omega_{ij}\Omega_{ji}} \tag{10c}$$

$$A_0 = 4.04 \tag{10d}$$

$$A_1 = \sqrt{6} \cos \left[\frac{1}{3} \cos^{-1} \left(\sqrt{6} \frac{S_{ij}S_{jk}S_{ki}}{(S_{ij}S_{ji})^{\frac{3}{2}}} \right) \right] \tag{10e}$$

$$S_{ij} = \frac{1}{2} \left(\frac{\partial u_i}{\partial x_j} + \frac{\partial u_j}{\partial x_i} \right) \tag{10f}$$

$$\Omega_{ij} = \frac{1}{2} \left(\frac{\partial u_i}{\partial x_j} - \frac{\partial u_j}{\partial x_i} \right) \tag{10g}$$

Where the u_g and u_p are the velocity component parallel and perpendicular to gravity respectively.

The inflow boundary conditions are:

$$u = U_\infty, v = 0, T = T_\infty, P = P_\infty, l = 4mm, I = 5\% \quad (11a)$$

$$k = \frac{3}{2} (U_\infty I)^2 \quad (11b)$$

$$\epsilon = C_\mu^{3/4} \frac{k^{3/2}}{l} \quad (11c)$$

The jet inflow boundary conditions are:

$$u = 0, v = U_S, T = T_S, P = P_\infty, l = 4mm, I = 5\% \quad (12a)$$

$$k = \frac{3}{2} (U_\infty I)^2 \quad (12b)$$

$$\epsilon = C_\mu^{3/4} \frac{k^{3/2}}{l} \quad (12c)$$

The upper boundary was taken to be symmetric to reduce the possibility of errors by the experimentally accurate no-slip condition. The upper boundary is very far from the jet and therefore should have negligible effect on the numerical result. The bottom of the wind tunnel is made up of 12 mm thick acrylic, while the test section is 25.4 mm thick acrylic. The external boundary conditions are iso-thermal with a temperature of T_∞ . The test section external temperature is iso-thermal of $\frac{1}{2} (T_S + T_\infty)$. The outflow boundary is a simple pressure outflow of P_∞ .

3.1. Simulation Validation

A simulation validation study was performed to verify the results of the simulations. Typical verification was performed including flow model, grid independence, and comparison with experimental results. The conditions of the simulation validation are shown in table 1.

The results from Spalart-Allmaras, $k - \epsilon$, and $k - \omega$ were compared and the three models have a similar trend. SA tends to be a bit off, but this is expected due to issues with this type of problem[6]. All of the values were normalized utilizing the following equations, where D is the width of the jet.

Parameter	Value
$U_{\infty} (m/s)$	2.0 ± 0.02
$U_S (m/s)$	2.0 ± 0.2
$T_{\infty} (K)$	305 ± 0.5
$P_{\infty} (kPa)$	101.3 ± 0.01
$T_S (K)$	350 ± 2.0

Table 1: Validation test conditions

Figure 2 shows a comparison of the flow models at $X = 4.75$.

$$\phi = \frac{T - T_{\infty}}{T_S - T_{\infty}} \quad (13a)$$

$$X = \frac{x}{D} \quad (13b)$$

$$Y = \frac{y}{D} \quad (13c)$$

$$V = \frac{U}{U_{\infty}} \quad (13d)$$

$$V_S = \frac{U_S}{U_{\infty}} \quad (13e)$$

Grid independence is demonstrated by testing the temperature at a few locations with various grid sizes and geometries, as shown in table 2. Very little variation in simulated temperature over such a wide variety of cell counts shows that the result is most likely grid independent. The grid employed is an unstructured hexagonal mesh with refinement located near the jet and down stream of the jet.

The final validation is comparing the simulation against the experiment. This is done in figure 3. The simulation matches the experiment closely, with the exception of very close to the wall. This is to be expected as the flow models used, even with enhanced wall effects, have difficulty perfectly modelling the near wall conditions.

4. Inverse Solution Methodology

The basis for the solution strategy was described in a paper by VanderVeer and Jaluria [2], which was originally intended to solve the inverse plume

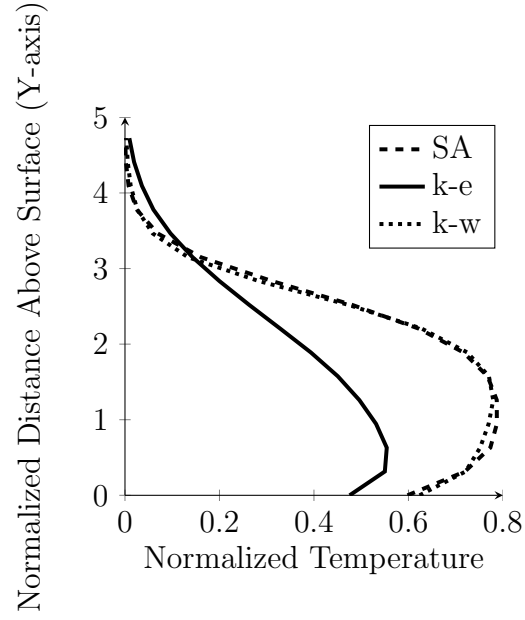


Figure 2: Validation of the simulation: local temperature using three flow models at $X = 4.75$

Location (x,y) (mm)	0,1	10,5	15,5	30,10
Cell Count				
57660	337.7	323.3	321.6	310.1
83888	337.7	323.3	321.6	310.1
166352	337.7	323.2	321.5	310.1
366168	337.7	323.2	321.5	310.1

Table 2: Grid Independence Study, local static temperature (K)

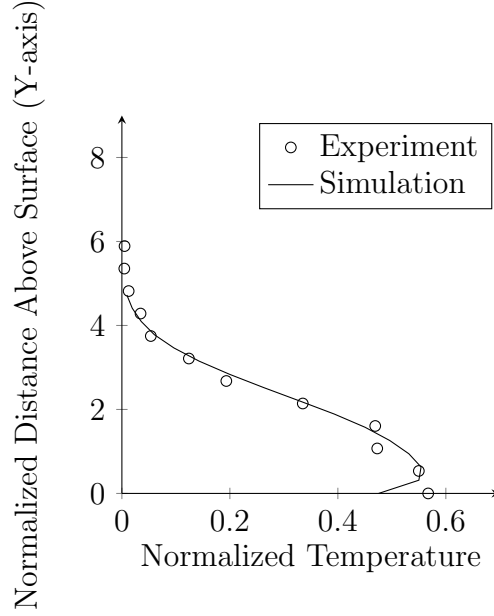


Figure 3: Validation of the simulation: local temperature - experiment versus simulation at $X = 4.75$

in a crosswind. This methodology solved for the 2-D location and source strength of a plume in a crossflow. The jet in a crossflow solver must handle one additional parameter, the jet velocity. Therefore the methodology is required to be modified. For completions sake, the original methodology will be briefly described here.

The method assumed that we can neglect the variations in density, thermal buoyancy, and thermal radiation. If this is true than the temperature of a given location ($T(\mathbf{r})$) is linearly dependent upon the source temperature(T_S) as shown in equation (14). The two parameters m and b are both location(\mathbf{r}) dependent and may be calculated knowing a unique set of simulations A and

B.

$$T_S = m(\mathbf{r}) T(\mathbf{r}) + b(\mathbf{r}) \quad (14a)$$

$$\mathbf{r} = r(x, y) \quad (14b)$$

$$\mathbf{r}_i = \mathbf{r}_0 + \Delta_i \quad (14c)$$

$$m(\mathbf{r}) = \frac{T_{SA} - T_{SB}}{T_A(\mathbf{r}) - T_B(\mathbf{r})} \quad (14d)$$

$$b(\mathbf{r}) = T_{SA} - m(\mathbf{r}) T_A(\mathbf{r}) \quad (14e)$$

A few quick terms to make the following explanation easier. Sample point: local static temperature from within the domain at a particular location. Datum point: a selected sample point whose location will be defined as $\Delta_0 = (0\text{ mm}, 0\text{ mm})$. Search shape: relative location and pattern between a set of sample points and a datum point.

Start by selecting n sample points and d simulations. The method attempts to minimize the discrepancies between all of the sample points' calculated source temperature and the datum point's calculated source temperature to get a predicted source temperature. Then minimize the discrepancy between the predicted source temperature and a new set of sample point calculated source temperatures to get the corrected location and temperature. The following equations mathematically describe the previous text. Equation (15) is minimized and the location \mathbf{r}_{SP}^* is used to calculate the predicted source temperature in equation (16). Then equation (17) is minimized and the location \mathbf{r}_{SP} is calculated with equation (18) used to calculate T_{SP} . Where a is the number of sample points used in the prediction step and n is the total number of sample points.

$$F(\mathbf{r}) = \sum_{i=1}^a [m(\mathbf{r} + \Delta_i) T(\mathbf{r}_i) + b(\mathbf{r} + \Delta_i) - m(\mathbf{r}) T(\mathbf{r}_0) - b(\mathbf{r})]^2 \quad (15)$$

$$T_{SP}^* = \frac{1}{a} \left\{ \sum_{i=0}^a [m(\mathbf{r}_{SP}^* + \Delta_i) T(\mathbf{r}_i) + b(\mathbf{r}_{SP}^* + \Delta_i)] \right\} \quad (16)$$

$$F_{mod}(\mathbf{r}) = \sum_{i=a}^n [m(\mathbf{r} + \Delta_i) T(\mathbf{r}_i) + b(\mathbf{r} + \Delta_i) - T_{SP}^*]^2 \quad (17)$$

$$T_{SP} = \frac{1}{n-a} \left\{ \sum_{i=a}^{n-a} [m(\mathbf{r}_{SP} + \Delta_i) T(\mathbf{r}_i) + b(\mathbf{r}_{SP} + \Delta_i)] \right\} \quad (18)$$

The number and pattern of the sample points (i.e. the search shape) was optimized in a paper by VanderVeer and Jaluria [3]. In it three sample points were identified as being enough to solve the inverse plume problem. The three points were later shown that they did not handle error very well and the optimization process was continued to include nine sample points. They are shown in table 3.

Sample Point	Δ (mm)
0	(0.0, 0.0)
1	(1.7, 3.5)
2	(2.8, 0.6)
3	(0.5, 1.1)
4	(2.1, 1.0)
5	(2.3, 2.0)
6	(1.2, 0.8)
7	(3.1, 0.7)
8	(0.8, 2.1)

Table 3: Search shape results of averaging over the domain with increasing the sample size to 9

Going back to the inverse jet in a crossflow problem, Knight et al. [7] used a quadratic response surface model to determine the jet temperature and jet velocity. While the response surface is not directly useful in finding the location, knowing the jet velocity is quadratic and the temperature is linear is.

The method starts similar to the original method, select n sample points and d simulations spanning the thermal and velocity region of interest. Guess a jet velocity (U_S) so the parameters are not dependent upon the jet velocity. Calculate the parameters m and b from equation (14). Find the minimization of equation (15) in which we can find a predicted equation (16). We can develop an equation similar to equation (15) for the jet velocity. Starting with equation (19), we can minimize the discrepancy between the predicted jet velocities resulting in equation (20). As would be expected there are three parameters needed ($\Gamma_0.. \Gamma_2$). The minimization of G allows to calculate U_S from equation (21). A flowchart of the methodology is shown in figure 4.

$$U_S = \Gamma_2(\mathbf{r}) T(\mathbf{r})^2 + \Gamma_1(\mathbf{r}) T(\mathbf{r}) + \Gamma_0(\mathbf{r}) \quad (19)$$

$$\begin{aligned} G(\mathbf{r}) = \sum_{i=a}^n & [\Gamma_2(\mathbf{r} + \Delta_i) T(\mathbf{r}_i)^2 \\ & + \Gamma_1(\mathbf{r} + \Delta_i) T(\mathbf{r}_i) \\ & + \Gamma_0(\mathbf{r} + \Delta_i) \\ & - \Gamma_2(\mathbf{r}) T(\mathbf{r}_0)^2 \\ & - \Gamma_1(\mathbf{r}) T(\mathbf{r}_0) \\ & - \Gamma_0(\mathbf{r})]^2 \end{aligned} \quad (20)$$

$$\begin{aligned} U_{SP} = \frac{1}{n-a} & \left\{ \sum_{i=a}^{n-a} [\Gamma_2(\mathbf{r}_{SP} + \Delta_i) T(\mathbf{r}_i)^2 \right. \\ & + \Gamma_1(\mathbf{r}_{SP} + \Delta_i) T(\mathbf{r}_i) \\ & \left. + \Gamma_0(\mathbf{r}_{SP} + \Delta_i)] \right\} \end{aligned} \quad (21)$$

5. Results and discussions

Due to the new methodology an incremental approach to solving the problem was used. Working from the simplest cases and move towards the more difficult cases, ending with the experimental results. Twenty-four selected cases are used to demonstrate the capabilities and weaknesses of the described methodology. The cases are labeled A-X, the conditions of the selected cases are described in table 4 with the constant parameters in table 5. For example, case T has a datum at 20 mm downstream, 3 mm above the surface, jet velocity of 1 m/s, and jet temperature of 425 K.

The next two steps utilize a single sample point, however, the rest use the nine sample points listed in table 3. The search shape used here is the optimized search shape for a plume with all nine sample points included. Utilizing a jet optimized search shape may yield better results.

5.1. Source Location and Velocity Known

The first condition of unknown source temperature, the methodology breaks down to a linear equation. Due to the simple linear equation a single sample point is needed to solve the inverse problem. The results of the selected cases are shown in figure 5. The error is typically less than 0.1%.

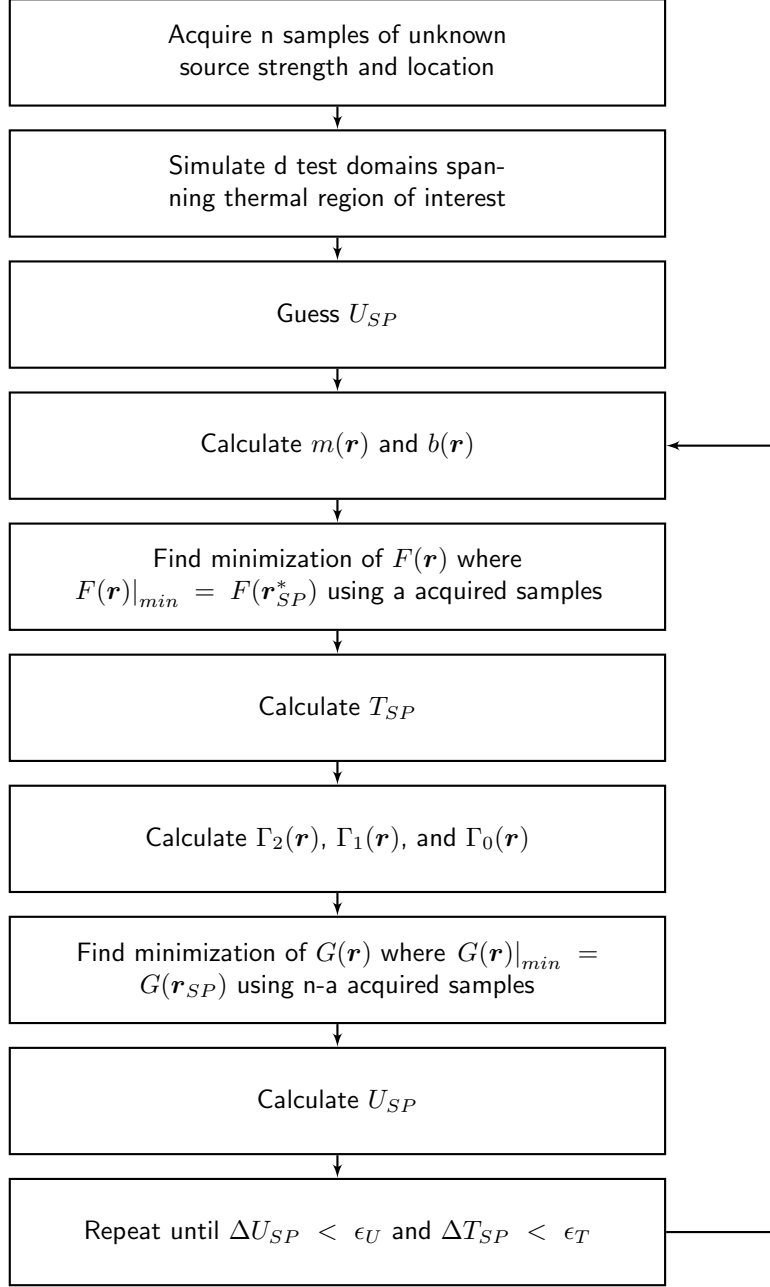


Figure 4: Flow chart of the predictor - corrector methodology for a jet in a crossflow

U_S (m/s)	1	1	2	2	4	4
T_S (K)	375	425	375	425	375	425
Location (x,y)						
10 mm, 1 mm	A	B	C	D	E	F
10 mm, 3 mm	G	H	I	J	K	L
20 mm, 1 mm	M	N	O	P	Q	R
20 mm, 3 mm	S	T	U	V	W	X

Table 4: Several sampled case parameters

Parameter	Value
U_∞ (m/s)	2
T_∞ (K)	293
P_∞ (kPa)	101.3

Table 5: Simulation test conditions

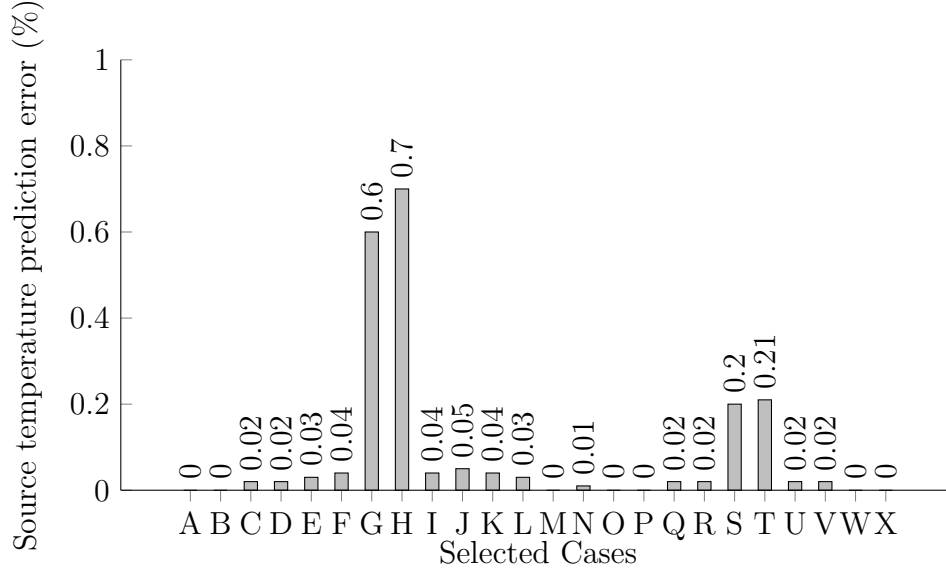


Figure 5: Error in the prediction of T_S from several sampled cases within the jet with r_S and U_S known

There are four cases with large error and they are located outside or near the edge of the jet. The temperature at these locations is near the ambient temperature and the Matlab polynomial curve fit has issues with the data points very similar to each other. The error is calculated using equation (22).

$$error_{temp}(\%) = \frac{|T_{SP} - T_S|}{T_S - T_\infty} \times 100 \quad (22a)$$

$$error_{x-location}(\%) = \frac{|x_{SP} - x_S|}{x_S} \times 100 \quad (22b)$$

$$error_{y-location}(\%) = \frac{|y_{SP} - y_S|}{y_S} \times 100 \quad (22c)$$

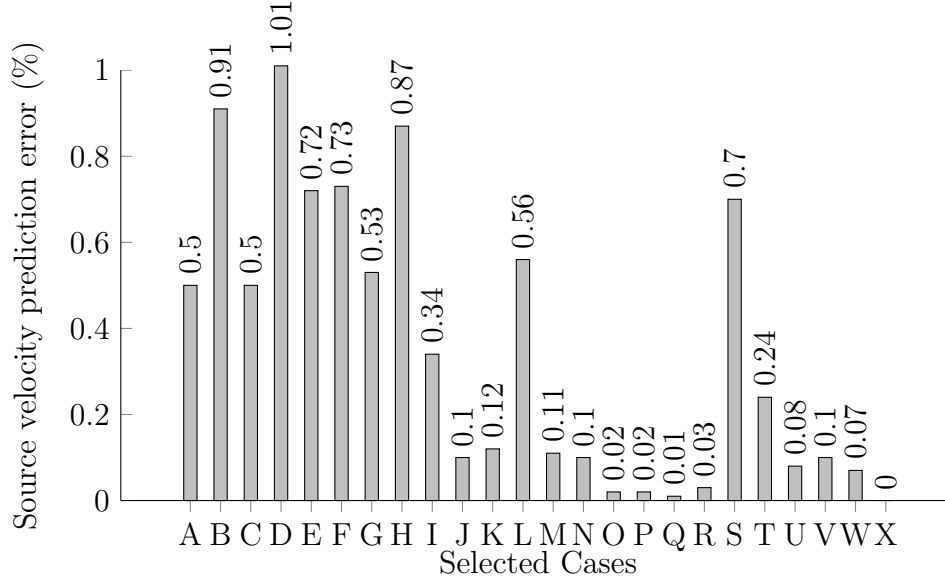


Figure 6: Error in the prediction of U_S from several sampled cases within the jet with r_S and T_S known

Axial Loc. (mm)	Elev. Loc. (mm)	Jet Temp. (K)	Jet Vel. (m/s)	Search Shape Error (%)
20.0	3.0	425	2.0	0.00
10.0	3.7	375	2.5	0.60
12.0	5.1	375	3.0	0.34
14.8	2.7	400	2.0	0.30
16.3	4.5	400	2.5	0.26
19.5	5.9	400	3.0	0.29
21.8	5.0	425	2.5	0.24
25.6	6.5	425	3.0	0.34
25.2	3.2	450	2.0	0.13
26.8	5.4	450	2.5	0.25

Table 6: Example alternative solutions

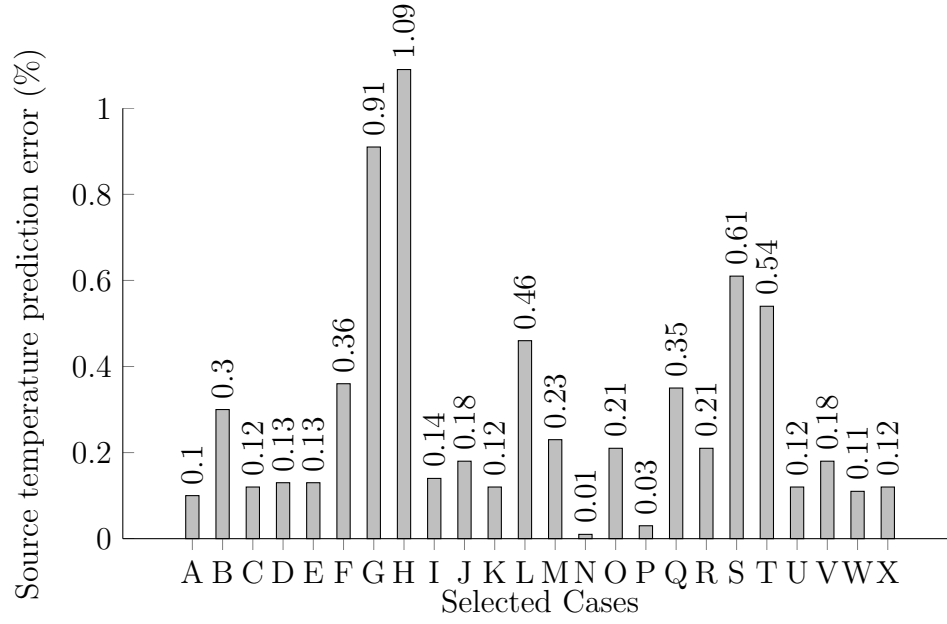


Figure 7: Error in the prediction of T_S from several sampled cases within the jet with r_S known

Parameter	Value
$T_\infty (K)$	297.6 ± 8.0
$P_\infty (kPa)$	100.6 ± 0.6
$U_\infty (m/s)$	2.0 ± 0.02

Table 7: Experimental test conditions

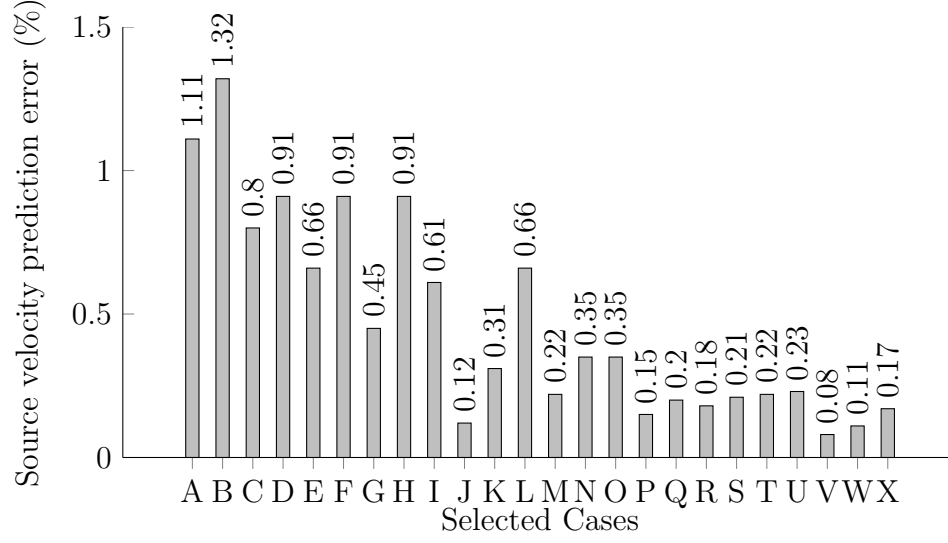


Figure 8: Error in the prediction of U_S from several sampled cases within the jet with r_S known

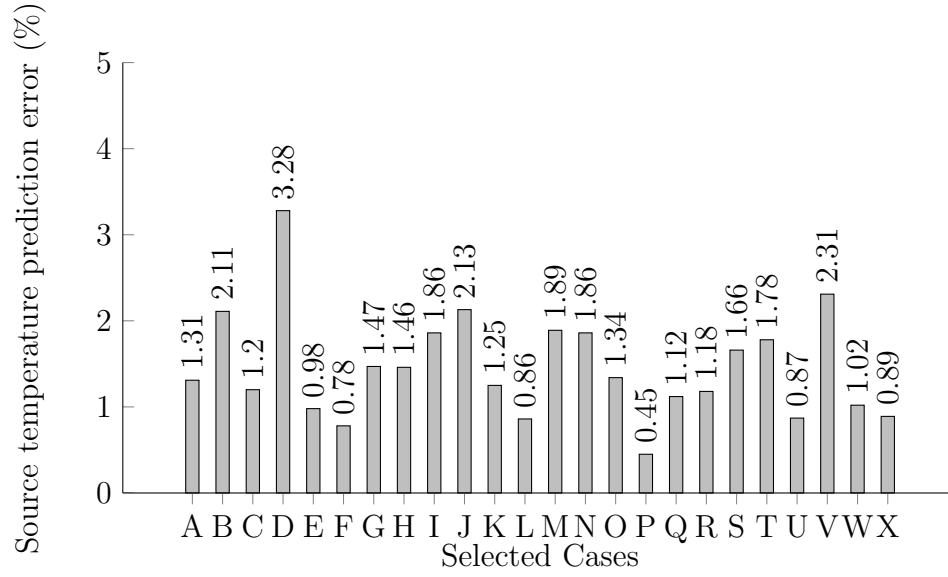


Figure 9: Error in the prediction of T_S from several sampled cases within the jet with source elevation known

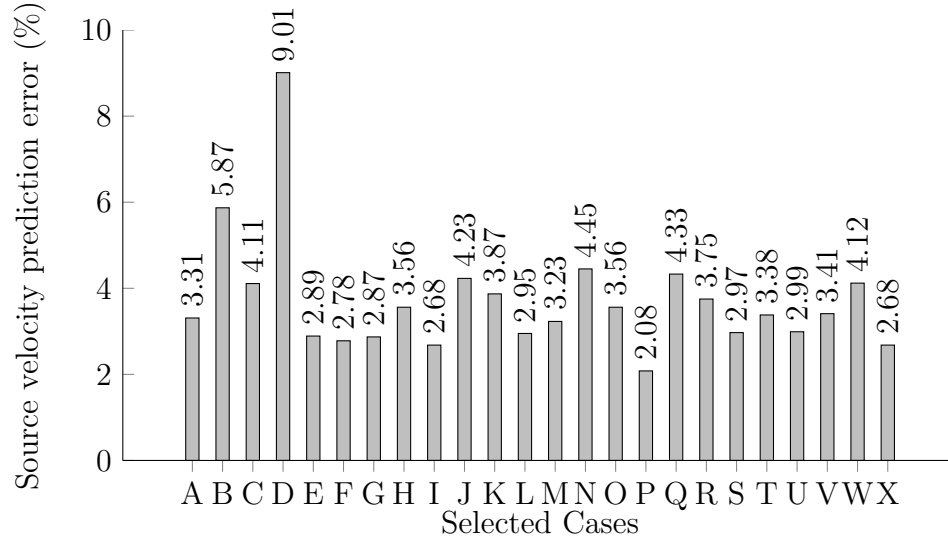


Figure 10: Error in the prediction of U_S from several sampled cases within the jet with source elevation known

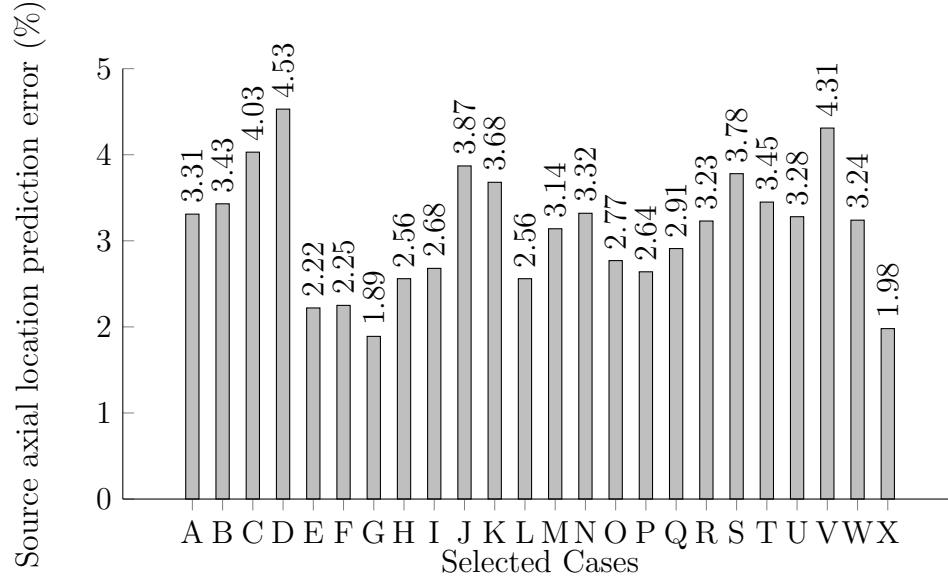


Figure 11: Error in the prediction of x_S from several sampled cases within the jet with source elevation known

U_S (m/s)		1.0	1.0	4.0	4.0
T_S (K)		375	425	375	425
Location (x,y)					
10 mm, 0 mm	X	10.9%	11.7%	11.1%	13.8%
	U	21.8%	18.6%	10.4%	11.9%
	T	8.70%	9.87%	10.7%	12.9%
20 mm, 0 mm	X	8.65%	7.65%	5.40%	9.81%
	U	18.7%	19.8%	11.5%	12.1%
	T	8.81%	10.7%	9.65%	10.2%
30 mm, 0 mm	X	10.6%	10.4%	18.7%	9.78%
	U	15.8%	17.9%	12.3%	13.7%
	T	9.61%	8.64%	13.7%	10.1%

Table 8: Error in predicting source axial location (x_S), source strength(U_S and T_S) from a few sample cases within the jet, search shape with 9pts, utilizing experimental data

5.2. Source Location and Temperature Known

5.3. Source Location Known

5.4. Source Elevation Known

5.5. Source Location and Strength Unknown

5.6. Experimental Results

6. Conclusions

References

- [1] J. Issa, Z. Yin, C. E. Polymeropoulos, Y. Jaluria, Temperature distribution in an optical fiber draw tower furnace, Journal of Materials Processing and Manufacturing Science vol 4 (1996) 221–232.
- [2] J. VanderVeer, Y. Jaluria, Solution of an inverse convection problem by a predictor-corrector approach, International Journal of Heat and Mass Transfer vol65 (2013) 123–130.
- [3] J. VanderVeer, Y. Jaluria, Optimization of an inverse convection solutions strategy, International Journal of Heat and Mass Transfer 73 (2014) 664–670.

- [4] Ansys, Fluent (version 13), 2010.
- [5] T. hsing Shih, W. Liou, A. Shabbir, Z. Yang, J. Zhu, A new $k - \epsilon$ eddy viscosity model for high reynolds number turbulent flows, Computer Fluids vol 24 (1995) 227–238.
- [6] Ansys, Fluent Technical Documents v14.0, Technical Report, Ansys, 2011.
- [7] D. Knight, Q. Ma, T. Rossmann, Y. Jaluria, Evaluation of fluid-thermal systems by dynamic data driven application systems - part ii, in: International Conference on Modeling and Optimization of Structures, Processes and Systems, Springer-Verlag, University of Kwazulu-Natal, South Africa, 2007.